

DNA Barcodes using a Cylindrical Nanopore

Swarnadeep Seth and Aniket Bhattacharya*

¹*Department of Physics, University of Central Florida, Orlando, Florida 32816-2385, USA*

(Dated: April 27, 2022)

We report an accurate method to determine DNA barcodes from the dwell time measurement of protein tags (barcodes) along the DNA backbone using Brownian dynamics simulation of a model DNA and use a recursive theoretical scheme which improves the measurements to almost 100% accuracy. The heavier protein tags along the DNA backbone introduce a large speed variation in the chain that can be understood using the idea of non-equilibrium tension propagation theory. However, from an initial rough characterization of velocities into “fast” (nucleotides) and “slow” (protein tags) domains, we introduce a physically motivated interpolation scheme that enables us to determine the barcode velocities rather accurately. Our theoretical analysis of the motion of the DNA through a cylindrical nanopore opens up the possibility of its experimental realization and carries over to multi-nanopore devices used for barcoding.

A DNA barcode consists of a short strand of DNA sequence taken from a targeted gene like COI or *cox I* (Cytochrome C Oxidase 1) [1] present in the mitochondrial gene in animals. The unique combination of nucleotide bases in barcode allows us to distinguish one species from another. Unlike relying on the traditional taxonomical identification methods, DNA barcoding provides an alternative and reliable framework to categorize a wide variety of specimens obtained from the natural environment. Though researchers relied on DNA sequencing techniques for the identification of unknown species for a long time, in 2003, Hebert *et al.* [2] proposed the mitochondrial gene (COI) region barcoding to classify cryptic species [3] from the entire animal population. Since then, several studies have shown the potential applications of barcoding in conserving biodiversity [4], estimating phyletic diversity, identifying disease vectors [5], authenticating herbal products [6], unambiguously labeling the food products [7, 8], and protecting endangered species [4]. Traditional sequencing methods based on chemical analysis are widely used in the biological community to determine the barcodes. Nanopore based sequencing methods [9] are being explored in a dual nanopore system for a cost effective, high throughput, chemical-free, and real time barcode generation.

The possibility of determining DNA barcodes have been demonstrated in a dual nanopore device, by scanning a captured dsDNA multiple times by applying a net periodic bias across the two pores [9–12]. Theoretical and simulation studies have also been reported in the context of a double nanopore system [13–15]. In this article, we investigate a similar strategy *in silico* in a cylindrical nanopore and demonstrate that a cylindrical nanopore can have a competitive advantage over a dual nanopore system. By studying a model dsDNA with barcodes using Brownian dynamics we establish an important result that it is due to the disparate dwell time and speed of

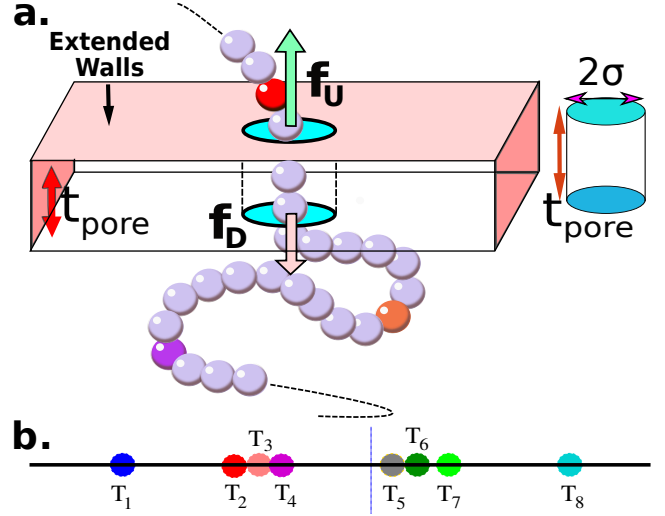


FIG. 1. Schematics of a model dsDNA captured in cylindrical nanopore of diameter $d = 2\sigma$ and thickness t_{pore} , where σ is the diameter of each monomer (purple beads). Protein tags (barcodes) of the same diameter but of different colors (only three are shown in here) interspersed along the dsDNA backbone. Opposite but unequal forces \vec{f}_U and \vec{f}_D are applied to straighten the dsDNA as it translocates in the direction bias net $\pm|\Delta\vec{f}_{UD}| = \pm|\vec{f}_U - \vec{f}_D|$ through the nanopore. (b) Positions of the protein tags along the contour length of the model dsDNA of length $L = 1024\sigma$ which represents an actual dsDNA of 48500 base pairs. The location of the tags are listed in Table-I.

the barcodes (“tags”) compared to the nucleotide segments (“monomers”) the current blockade time informa-

TABLE I. Tag positions along the dsDNA

Tag #	T_1	T_2	T_3	T_4	T_5	T_6	T_7	T_8
Position	154	369	379	399	614	625	696	901
Separation	154	215	10	20	215	11	71	205

* Author to whom the correspondence should be addressed; Aniket.Bhattacharya@ucf.edu

tion only is not enough and will lead to an inevitable underestimation of the distance between the barcodes.

Furthermore, using the ideas of the tension propagation theory [16, 17], we demonstrate that information about the fast-moving nucleotides in between the barcodes, - not easily accessible experimentally is a key element to resolve the underestimation. We suggest how to obtain this information experimentally and provide a physically motivated “two-step” interpolation scheme for an accurate determination of barcodes, even when the separation of (unknown) tags has a broad distribution.

- *The Model System:* Our *in silico* coarse-grained (CG) model of a dsDNA consist of 1024 monomers interspersed with 8 barcodes at different locations shown in Fig. 1 and Table-I is motivated by an experimental study by Zhang *et al.* on a 48500 bp long dsDNA with 75 bp long protein tags at random locations along the chain [10–12] using a dual nanopore device. Here we explore if a cylindrical nanopore with applied biases at each end can resolve the barcodes with similar accuracy or better. We purposely choose positions of the 8 barcodes (Table-I) to study how the effect of disparate distances among the barcodes affects their measurements. The tags T_2, T_3, T_4 are closely spaced and form a group. Likewise, another group consisting of T_5 and T_6 are put in a closer proximity to T_7 . The tags T_1 and T_8 are further apart from the rest of the tags. The general scheme of the BD simulation strategy for a translocating homo-polymer under alternate bias has been discussed in our recent publication [13, 14] and in the Appendix A.

In this article, tags are introduced by choosing the mass and friction coefficient at tag locations to be different than the rest of the monomers along the chain. This requires modification of the BD algorithm as discussed in the Appendix A. The protein tags used in the experiments [10–12] translate to about three monomers in the simulation. The heavier and extended tags introduce a larger viscous drag. Instead of explicitly putting side-chains at the tag locations, we made the mass and the friction coefficient of the tags 3 times larger. This we find enough to resolve the distance between the tags. Two forces \vec{f}_U and \vec{f}_D at each end of the cylinder in opposite directions keep the DNA straight inside the channel and allows translocation in the direction of the net bias (please see Fig. 1 and Fig. 2).

- *Barcodes from repeated scanning:* As potentially could be done in a nanopore experiments, we switch the differential bias once the first tag or the last tag (T_1 , T_8) translocates through the nanopore during up(U)/down(D) \rightarrow D/U translocation yet having end segments inside the pore (please see Fig. 2) so that the DNA remains captured in the cylindrical pore and the barcodes are scanned multiple times. The question we ask: can we recover the actual barcode locations from these scanning measurements, so that the method can be applied to determine unknown barcodes? We monitor two important quantities, - the dwell time of each

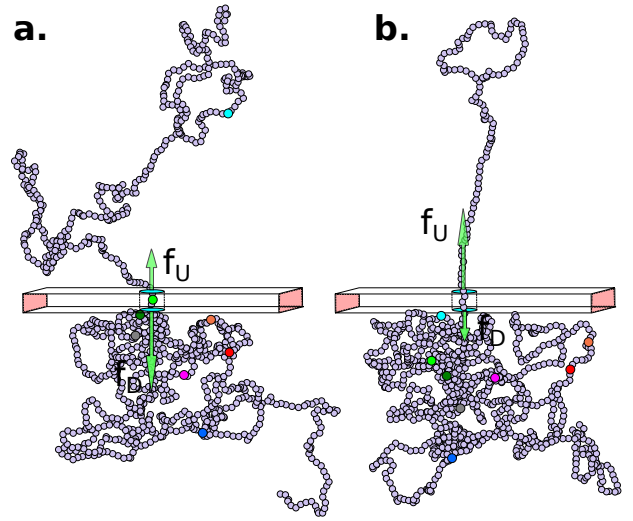


FIG. 2. Demonstration of the epoch when the bias voltage is flipped. (a) showing the last barcode is yet to translocate in the downward direction when the net bias $\Delta\vec{f}_{DU} = \vec{f}_D - \vec{f}_U > 0$. (b) shows the situation after a later time when finally all the barcodes crossed the cylindrical pore during downward translocation with a portion of the end segment still remaining inside the pore. At this point the bias is flipped with an upward bias $\Delta\vec{f}_{UD} = \vec{f}_U - \vec{f}_D > 0$, translocation now occurs in the upward direction. In this way, the DNA remains captured all the time during repeated scans.

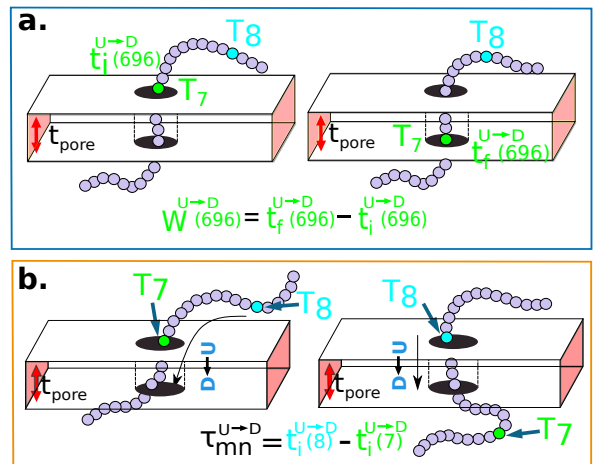


FIG. 3. (a) Demonstration of calculation of wait time for T_7 which has the monomer of index $m = 696$. The dwell velocity is then calculated using Eqn. 2. (b) Demonstration of calculation of tag time delay $\tau_{78}^{U \rightarrow D} = t_i^{U \rightarrow D}(8) - t_i^{U \rightarrow D}(7)$ for tags T_7 and T_8 while they are moving downward. Please note that similar quantity for upward translocation $\tau_{87}^{D \rightarrow U} = t_i^{D \rightarrow U}(7) - t_i^{D \rightarrow U}(8) \neq \tau_{78}^{U \rightarrow D}$ as there is no symmetry of the tags along the chain.

monomer and the time delay of arrival of two successive monomers at the pore as demonstrated in Fig. 3 and explained below. For each up/down-ward scan we measure

the dwell times of the monomer m as follows:

$$W^{U \rightarrow D}(m) = t_f^{U \rightarrow D}(m) - t_i^{U \rightarrow D}(m), \quad (1a)$$

$$W^{D \rightarrow U}(m) = t_f^{D \rightarrow U}(m) - t_i^{D \rightarrow U}(m). \quad (1b)$$

Here $t_i^{U \rightarrow D}(m)$ and $t_f^{U \rightarrow D}(m)$ are the arrival and exit times of the monomer with index m as further demonstrated in Fig. 3(a). The corresponding dwell velocities $v_{dwell}^{U \rightarrow D}(m)$ and $v_{dwell}^{D \rightarrow U}(m)$ for the m^{th} bead (either a monomer or a tag) along the channel axis (please see Fig. 3(a)) can be obtained as follows.

$$v_{dwell}^{U \rightarrow D}(m) = t_{pore}/W^{U \rightarrow D}(m), \quad (2a)$$

$$v_{dwell}^{D \rightarrow U}(m) = t_{pore}/W^{D \rightarrow U}(m). \quad (2b)$$

In an actual experiment one measures the dwell velocities of the tags only which are equivalent to the current blockade times.

- *Non uniformity of the dwell velocity:* The presence of tags with heavier mass ($m_{tag} = 3m_{bulk}$) and larger solvent friction ($\gamma_{tag} = 3\gamma_{bulk}$) introduces a large variation in the dwell time and hence a large variation in the dwell velocities of the DNA beads and tags (see Fig. 4). In general, there is no up-down symmetry for the dwell time/velocity as tags are not located symmetrically along the chain backbone. Thus the physical quantities are averaged over $U \rightarrow D$ and $D \rightarrow U$ translocation data. The average dwell velocity $\bar{v}_{dwell}(m) = \frac{1}{2} [v_{dwell}^{U \rightarrow D}(m) + v_{dwell}^{D \rightarrow U}(m)]$ clearly shows two different velocity envelopes - the tags residing at the lower envelope. Fig. 4 shows that the dwell velocities of the tags (green

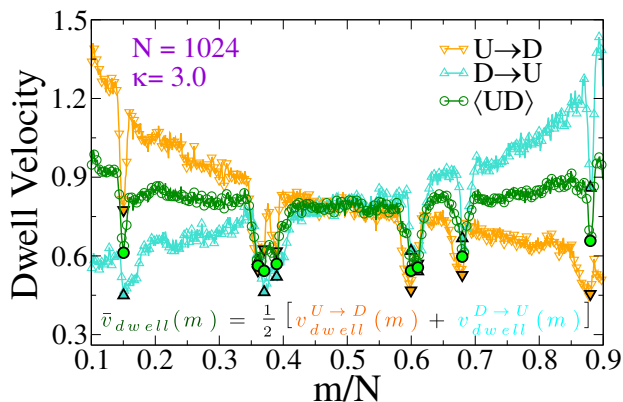


FIG. 4. Dwell velocity of monomer in a cylindrical nanopore system. ∇ and \triangle represent downward and upward translocation. \circ are average of both directions. Filled triangles and circles correspond to tag dwell velocities.

circle \bullet) are significantly lower than the velocity of the nucleotides in between the tags, which will underestimate the barcode distances as explained later. We further notice that increasing the pore width resolves the barcodes better.

- *Barcode estimation using a cylindrical nanopore setup:* If the dsDNA with barcodes were a rigid rod, then

one could obtain the barcode distances $d_{mn}^{U \rightarrow D}$ and $d_{nm}^{D \rightarrow U}$ between tags T_m and T_n from the following equations (shown for downward translocation only):

$$d_{mn}^{U \rightarrow D} = v_{mn}^{U \rightarrow D} \times \tau_{mn}^{U \rightarrow D} \quad \text{where,} \quad (3a)$$

$$v_{mn}^{U \rightarrow D} = \frac{1}{2} [v_{dwell}^{U \rightarrow D}(m) + v_{dwell}^{U \rightarrow D}(n)], \quad (3b)$$

$$\tau_{mn}^{U \rightarrow D} = (t_i^{U \rightarrow D}(n) - t_i^{U \rightarrow D}(m)). \quad (3c)$$

Here $\tau_{mn}^{U \rightarrow D}$ is the time delay of arrivals of T_m and T_n for downward translocation (please see Fig. 3(b) which explains the special case when $m = 7$ and $n = 8$). Similar Equations can be obtained by flipping D and m with U and n respectively. In other words, Eqn. 3 gives the shortest distance and not necessarily the contour length (the actual distance) between the tags. However, this is the only data accessible through experiments and likely to provide an underestimation of the barcodes. Fig. 5(a) shows the data for 300 scans. The average with error bars are shown in the 3rd column of Table-II. Excepting for T_6 these measurements grossly underestimate the actual positions with large error bars.

TABLE II. Barcodes from various methods

Tag Label	Relative Distance w.r.t T_5	Barcode (Eqn. 3)	Barcode (Method-I)	Barcode (Method-II)
T_1	460	373 \pm 122	459 \pm 59	460 \pm 43
T_2	245	197 \pm 67	250 \pm 39	250 \pm 32
T_3	235	183 \pm 63	237 \pm 38	237 \pm 32
T_4	215	167 \pm 54	211 \pm 35	211 \pm 30
T_5	0	0	0	0
T_6	11	11 \pm 3	14 \pm 4	11 \pm 3
T_7	82	68 \pm 23	86 \pm 23	86 \pm 21
T_8	287	230 \pm 73	287 \pm 65	287 \pm 73

- *Tension Propagation (TP) Theory explains the source of discrepancy and provides solution:* Unlike a rigid rod, tension propagation governs the semi-flexible chain's motion in the presence of an external bias. In TP theory and its implementation in Brownian dynamics, the motion of the subchain in the *cis* side decouples into two domains [16, 17]. In the vicinity of the pore, the tension front affects the motion directly while the second domain remains unperturbed, beyond the reach of the TP front. In our case, after the tag T_m translocates through the pore, preceding monomers are dragged into the pore quickly by the tension front, analogous to the uncoiling effect of a rope pulled from one end. The onset of this sudden *faster* motion continues to grow and reaches its maximum until the tension front hits the subsequent tag $T_{m\pm 1}$, with larger inertia and viscous drag. At this time (called the tension propagation time [18]) the faster motion of the monomers begins to taper down to the velocity of the tag $T_{m\pm 1}$. This process continues from one segment to the other. Fig. 6 shows an example on how the segment connecting T_7 and T_8 has non-monotonic velocity under the influence of the tension front. These

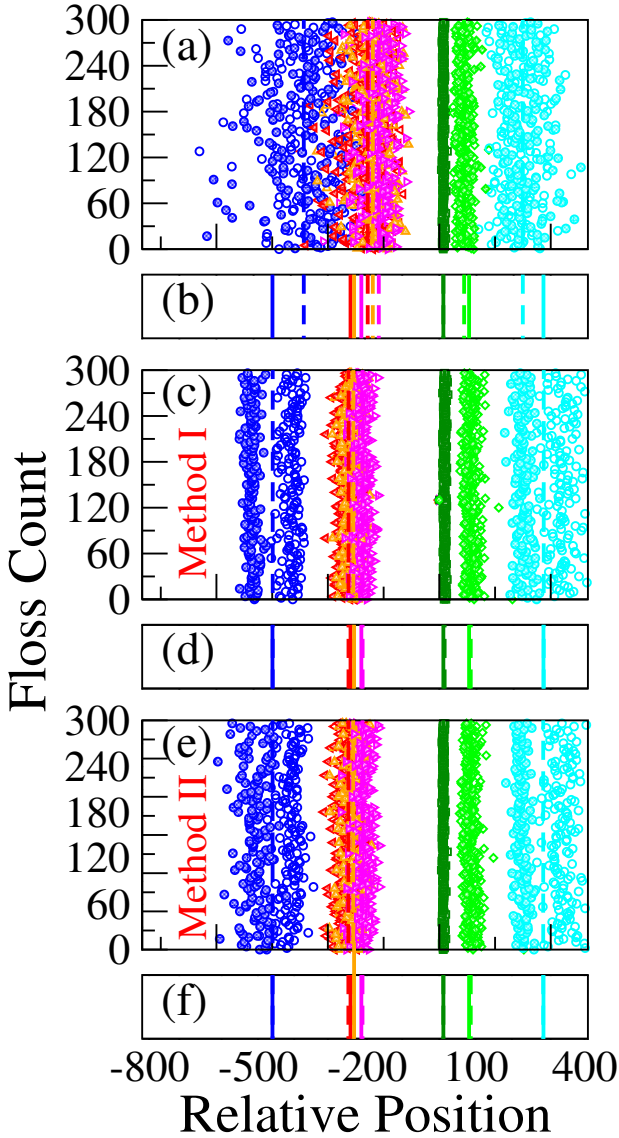


FIG. 5. (a) Barcodes generated using different methods. In each graph, the colored symbols/lines refer to the corresponding colors of the barcodes T_1 , T_2 , T_3 , T_4 , T_5 , T_6 , T_7 , and T_8 respectively. The open and filled symbols represent barcodes for $U \rightarrow D$ and $D \rightarrow U$ translocation using (a) Eqn. 3; (c) using method 1, and (e) using method 2. In (b), (d) and (e) the solid lines refer to the actual location of the barcodes and the dashed lines correspond to the averages from (a), (c) and (e) respectively. The improved accuracy for the latter two methods are readily visible in (d) and (f) where the simulation and the actual data are almost indistinguishable.

contour lengths of faster moving segments in between two barcodes are not accounted for in Eqn 3. The experimental protocols are limited in extracting barcode information through Eqn. 3 (measuring current blockade time) and therefore, likely to underestimate the barcodes, unless the data is corrected to account for the faster moving monomers in between two tags.

- *How to determine the barcodes correctly?* Fig. 1(b)

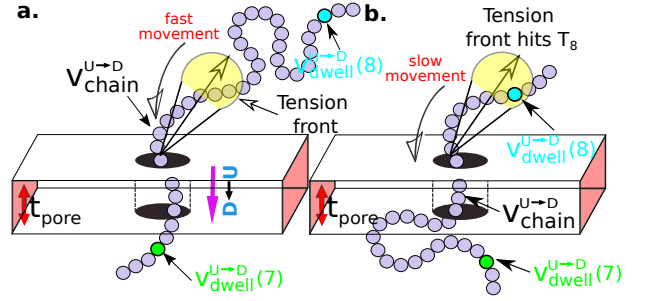


FIG. 6. Tension propagation (TP) through the chain backbone connecting T_7 and T_8 . (a) Figure shows a sudden fast movement of monomers right after T_7 's passage through the pore. Due to the TP front's influence (yellow blob region), subsequent monomers are sucked into the pore quickly. (b) TP front finally reaches T_8 , leading to a slower translocation speed due to the tag's large inertia and higher viscous drag.

and the 3rd column of Table-II when looked closely provide clues to the solution of the underestimated tag distances. We note that locations of the isolated tags (such as, T_1 and T_8) far from T_5 have a larger error bar while T_6 which is adjacent to T_5 has the correct distance from Eqn. 3. It is simply because in the later case the contour length between T_5 and T_6 is almost equal to the shortest distance. Evidently, the error bars increase with increased separation.

To compare the barcodes obtained from Eqn. 3 with the actual contour length (see 2nd column of Table-II) between tag pairs, we invoke the Flory theory to determine the scaling exponent ν [19] which reveals the behavior of the segments under translocation. The heatmap in Fig. 7 confirms that when the separation between the tag pairs is less compared to the DNA length, the connecting segment behaves like a rigid rod ($\nu > 0.6$). While for the isolated tags, $\nu < 0.6$ suggests that barcodes are shorter than their respective contour lengths. This clarifies the reason behind the barcode underestimation for the tags which are spaced apart while yielding accurate barcodes for tags located in groups.

Within the experimental set up we suggest the following two methods which will account for the larger velocities of the monomers.

Method 1 - Barcode from known end-to-end Tag distance: In order to measure the barcode distances accurately one thus needs the velocity of the entire chain. If the distance between T_1 and T_8 $d_{18} \simeq L$, then the velocity of the segment d_{18} will approximately account for the average velocity of the entire chain v_{chain} and correct the problem as demonstrated next. First we estimate the velocity of the chain

$$v_{chain}^{U \rightarrow D} \approx v_{18}^{U \rightarrow D} = d_{18} / \tau_{18}^{U \rightarrow D}, \quad (4)$$

assuming we know d_{18} and $\tau_{18}^{U \rightarrow D}$ is the time delay of arrival at the pore between T_1 and T_8 for $U \rightarrow D$ translocation. We then estimate the barcode distance $d_{mn}^{U \rightarrow D}$

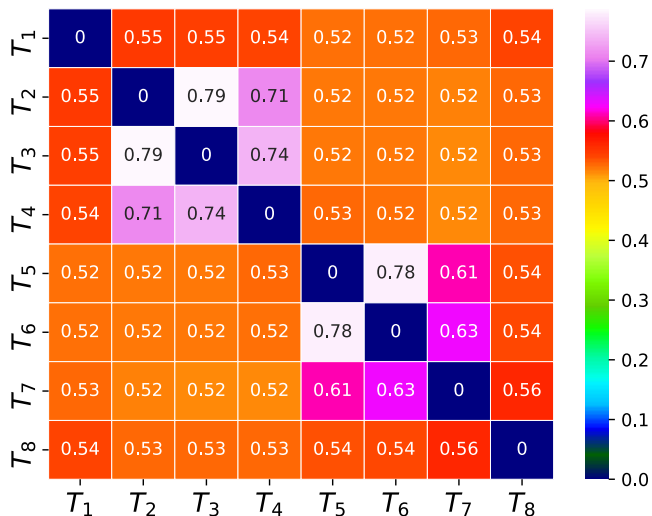


FIG. 7. Flory exponent (ν) for the segment connecting a tag pair represented as a two dimensional heatmap array on the color scale ranging from blue to white.

between tags T_m and T_n as

$$d_{mn}^{U \rightarrow D} = v_{18}^{U \rightarrow D} \times \tau_{mn}^{U \rightarrow D}. \quad (5)$$

In the similar fashion one can calculate $d_{mn}^{D \rightarrow U}$ using $v_{chain}^{D \rightarrow U}$ and $\tau_{mn}^{D \rightarrow U}$ information respectively. How do we know d_{18} ? One can use $d_{18} \approx L_{scan}$ and $v_{chain} \approx \bar{v}_{scan}$, from Eqn. 6 where \bar{v}_{scan} is the the average velocity of the scanned length L_{scan} from repeated scanning as discussed in the next paragraph. This method is effective for estimating the long-spaced barcodes but it overestimates the barcode distance if multiple barcodes are close by as evident in Fig. 5(d) and the 4th column of table-II. Thus, we know how to obtain barcode distances accurately when they are close by (from Eqn. 3) and for large separation (Eqn. 5). We now apply the physics behind these two schemes to derive an interpolation scheme that will work for all separations among the barcodes.

Method 2 - Barcode using two-step method: Average scan time $\bar{\tau}_{scan}$ for the entire chain (which can be measured experimentally) is a better way to estimate the average velocity of the chain. L_{scan} is the maximum length up to which the dsDNA segment remains captured inside the nanopore gets scanned and denotes the theoretical maximum beyond which the dsDNA will escape from the nanopore, thus, $L \approx L_{scan}$. For example, in our simulation, scanning length $L_{scan} = 0.804L$. We denote the average scan velocity as

$$\bar{v}_{scan} = \frac{1}{N_{scan}} \sum_{i=1}^{N_{scan}} L_{scan} / \tau_{scan}(i), \quad (6)$$

where $\tau_{scan}(i)$ is the scan time for the i^{th} event, and $N_{scan} = 300$. To proceed further, we use our established results that the monomers of the dsDNA segments in between the tags move with velocity \bar{v}_{scan} , while tags move

with their respective dwell velocities $v_{mn}^{U \rightarrow D}$ and $v_{mn}^{D \rightarrow U}$ (Eqn. 2). We then calculate the segment velocity between two tags by taking the *weighted average* of the velocities of tags and DNA segment in between as follows.

First, we estimate the approximate number of monomers $N_{mn} = d_{mn}^{U \rightarrow D} / \langle b_l \rangle$ ($\langle b_l \rangle$ is the bond-length) by considering the tag velocities only using Eqn. 3. We then calculate the segment velocity accurately by incorporating weighted velocity contributions from both the tags and the monomers between the tags.

$$v_{weight}^{U \rightarrow D} = \frac{1}{N_{mn}} \left[v_{dwell}^{U \rightarrow D}(m) + v_{dwell}^{U \rightarrow D}(n) + (N_{mn} - 2)\bar{v}_{scan} \right] \quad (7)$$

The barcodes are finally estimated by multiplying the calculated 2-step velocity in Eqn. 7 above by the tag time delay as

$$d_{mn}^{U \rightarrow D} = v_{weight}^{U \rightarrow D} \times \tau_{mn}^{U \rightarrow D} \quad (8)$$

for $U \rightarrow D$ translocation and repeating the procedure for $D \rightarrow U$ translocation. This 2-step method accurately captures the distance between the barcodes when the two tags are in proximity or spaced apart from each other. Table-II and Fig. 5 summarize our main results and claims.

- *Summary & Future work:* Motivated by the recent experiments we have designed barcode determination experiment *in silico* in a cylindrical nanopore using the Brownian dynamics scheme on a model dsDNA with known locations of the barcodes. We have carefully chosen the locations of the barcodes so that the separations among the barcodes span a broad distribution. We discover that if we use the dwell time data only for the barcodes from multiple scans of the dsDNA to calculate the average velocities of the tags then the method underestimates the barcode distances for tags further apart. Our simulation guides us to conclude that the source of this underestimation lies in neglecting the information contained in the faster moving DNA segments in between any two tags. We use non-equilibrium tension propagation theory to explain the non-monotonic velocity of the chain segments where the barcodes lie at the lower bound of the velocity envelope as shown in Fig. 4. The emerging picture readily shows the way how to rectify this error by introducing an interpolation scheme that works well to determine barcodes spaced apart for all distances which we validate using simulation data. We suggest how to implement the scheme in an experimental setup. It is important to note that the interpolation scheme-based concept of the TP theory is quite general and we have ample evidence that this will work in a double nanopore system as well.

- *Conflicts of interest:* The authors declare no competing financial interest.

- *Acknowledgements:* The research at UCF has been supported by the grant number 1R21HG011236-01 from

the National Human Genome Research Institute at the National Institute of Health. All computations were carried out at the UCF's high performance computing platform STOKES.

Appendix A: The Model and Brownian dynamics simulation

Our BD scheme is implemented on a bead-spring model of a polymer with the monomers interacting via an excluded volume (EV), a Finite Extension Nonlinear Elastic (FENE) spring potential, and a bond-bending potential enabling variation of the chain persistence length ℓ_p (Fig.A1). The model, originally introduced for a fully flexible chain by Grest and Kremer [20], has been studied quite extensively by many groups using both Monte Carlo (MC) and various molecular dynamics (MD) methods [21]. Recently we have generalized the model for a semi-flexible chain and studied both equilibrium and dynamic properties [18, 22, 23] and studied compression dynamics of a model dsDNA inside a nanochannel [24, 25]. The mutual EV interaction among any two monomers are given by the truncated Lennard-Jones (LJ) potential with a cut-off radius $2^{1/6}\sigma$

$$U_{LJ}(r_{ij}) = \begin{cases} 4\epsilon \left[\left(\frac{\sigma}{r_{ij}} \right)^{12} - \left(\frac{\sigma}{r_{ij}} \right)^6 \right] + \epsilon, & \text{for } r < 2^{1/6}\sigma \\ 0, & \text{otherwise} \end{cases} \quad (\text{A1})$$

where σ is the effective diameter of a monomer and ϵ is the interaction strength. To mimic the connectivity between two adjacent monomers, finite-extensible-nonlinear elastic (FENE) potential

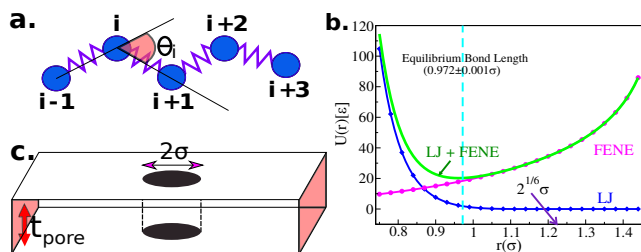


FIG. A1. (a) Illustration depicts the monomers are interacting via LJ and FENE potential. The three body bending potential is calculated using the angle θ_i between two adjacent bond vectors \vec{b}_i and \vec{b}_{i+1} respectively. (b) Interaction potential between two consecutive monomers is given by the green line for a separation distance r in unit of σ . The blue diamonds denote the LJ potential with a cutoff radius $2^{1/6}\sigma$ and the magenta circles correspond to the FENE potential with a spring constant $\kappa_F = 30.0\epsilon/\sigma^2$. (c) A cylindrical nanopore of diameter 2σ is drilled into a material of thickness t_{pore} . The walls consist of purely repulsive LJ particles.

$$U_{FENE}(r_{ij}) = -\frac{1}{2}\kappa_F R_0^2 \ln \left[1 - \left(\frac{r_{ij}}{R_0} \right)^2 \right] \quad (\text{A2})$$

is used with the maximum bond-stretching length $R_0 = 1.5\sigma$ and spring constant $\kappa_F = 30\epsilon/\sigma^2$. Here, $r_{ij} = |\vec{r}_i - \vec{r}_j|$ is the separation distance between two adjacent monomers i and $j = i \pm 1$ located at \vec{r}_i and \vec{r}_j respectively. Along with these two potentials, we introduce a bending potential

$$U_{bend}(\theta_i) = \kappa (1 - \cos(\theta_i)) \quad (\text{A3})$$

with bending rigidity κ . In three dimensions, for $\kappa \neq 0$, the persistence length ℓ_p of the chain is related to κ via [26]

$$\ell_p = \frac{\kappa}{k_B T}, \quad (\text{A4})$$

where k_B is the Boltzmann constant and T is the temperature. Here θ_i is the bond angle between two subsequent bond vectors $\vec{b}_i = \vec{r}_{i+1} - \vec{r}_i$ and $\vec{b}_{i-1} = \vec{r}_i - \vec{r}_{i-1}$. A cylindrical nanopore of diameter 2σ is drilled through a solid material of thickness t_{pore} consists of immobile and purely repulsive LJ particles. Our model of DNA polymer consists 1016 monomer beads along with 8 heavier tags ($T_1 - T_8$) located at positions 154, 369, 379, 399, 614, 625, 696, and 901 respectively (please refer to Fig. 2 and Table-I in the main article). A recent study by Zhang et al. on 48512 bp long dsDNA uses 75 bp long protein tags as barcodes [10]. In simulation, we purposely choose the mass of a tag (m_{tag}) three times heavier of a normal monomer to replicate the tags used in the experiments. We proportionally increase the solvent friction of the tags $\Gamma_{tag} = 3\Gamma_i$. We use the Brownian dynamics to solve the equation of motion of a monomer i having a mass m_i and solvent friction Γ_i as

$$m_i \ddot{\vec{r}}_i = \vec{\nabla}_i [U_{LJ} + U_{FENE} + U_{bend} + U_{wall}] - \Gamma_i \vec{v}_i + \eta_i \quad (\text{A5})$$

where $\Gamma_i = 0.7\sqrt{m_i\epsilon^2/\sigma^2}$ is the frictional coefficient arising from solvent-monomer interaction. For the case of a tag, $m_{tag} = 3m_i$ and $\Gamma_{tag} = 2.1\sqrt{m_i\epsilon^2/\sigma^2}$. The Gaussian white noise η_i arising from thermal fluctuation is delta correlated and expressed as $\langle \eta_i(t) \cdot \eta_j(t') \rangle = 2dk_B T \Gamma \delta_{ij} \delta(t - t')$ with $d = 3$ in three dimension. We express length and energy in units of σ and ϵ respectively such that $k_B T/\epsilon = 1.0$. The parameters for FENE potential in Eq. (A2) are κ_F and R_0 , and set to be $\kappa_F = 30\epsilon/\sigma^2$ and $R_0 = 1.5\sigma$. The numerical integration of Eq. (A5) is implemented using the algorithm introduced by Gunsteren and Berendsen [27]. Our previous experiences with BD simulation suggests that for a time step $\Delta t = 0.01$ these parameters values produce stable trajectories over a very long period of time and do not lead to unphysical crossing of a bond by a monomer [22, 23]. The average

bond length stabilizes to $\langle b_l \rangle = 0.971 \pm 0.001\sigma$ with negligible fluctuation regardless of the chain size and rigidity [22]. Hence we relate the polymer's contour length L

and the number of monomers N as $L = (N - 1)\langle b_l \rangle$.

-
- [1] Hebert, P. D. N.; Ratnasingham, S.; de Waard, J. R. Barcoding Animal Life: Cytochrome c Oxidase Subunit 1 Divergences among Closely Related Species. *Proc. R. Soc. Lond. B* **2003**, 270, 96.
- [2] Hebert, P. D. N.; Cywinska, A.; Ball, S. L.; deWaard, J. R. Biological Identifications through DNA Barcodes. *Proc. R. Soc. Lond. B* **2003**, 270 (1512), 313-321.
- [3] Hebert, P. D. N.; Penton, E. H.; Burns, J. M.; Janzen, D. H.; Hallwachs, W. Ten Species in One: DNA Barcoding Reveals Cryptic Species in the Neotropical Skipper Butterfly *Astraptes Fulgerator*. *Proceedings of the National Academy of Sciences* **2004**, 101 (41), 14812-14817.
- [4] Vernooij, R.; Haribabu, E.; Muller, M. R.; Vogel, J. H.; Hebert, P. D. N.; Schindel, D. E.; Shimura, J.; Singer, G. A. C. Barcoding Life to Conserve Biological Diversity: Beyond the Taxonomic Imperative. *PLoS Biol* **2010**, 8 (7), e1000417.
- [5] Besansky, N. J.; Severson, D. W.; Ferdig, M. T. DNA Barcoding of Parasites and Invertebrate Disease Vectors: What You Don't Know Can Hurt You. *Trends in Parasitology* **2003**, 19 (12), 545-546.
- [6] Techen, N.; Parveen, I.; Pan, Z.; Khan, I. A. DNA Barcoding of Medicinal Plant Material for Identification. *Current Opinion in Biotechnology* **2014**, 25, 103-110.
- [7] Xiong, X.; Yuan, F.; Huang, M.; Lu, L.; Xiong, X.; Wen, J. DNA Barcoding Revealed Mislabeling and Potential Health Concerns with Roasted Fish Products Sold across China. **2019**, 82 (7), 1200-1209.
- [8] Wong, E. H.-K.; Hanner, R. H. DNA Barcoding Detects Market Substitution in North American Seafood. *Food Research International* **2008**, 41 (8), 828-837.
- [9] Pud, S.; Chao, S.-H.; Belkin, M.; Verschuere, D.; Huijben, T.; van Engelenburg, C.; Dekker, C.; Aksimentiev, A. Mechanical Trapping of DNA in a Double-Nanopore System. *Nano Lett.* **2016**, 16 (12), 8021-8028.
- [10] Zhang, Y.; Liu, X.; Zhao, Y.; Yu, J.-K.; Reisner, W.; Dunbar, W. B. Single Molecule DNA Resensing Using a Two-Pore Device. *Small* **2018**, 14 (47), 1801890.
- [11] Liu, X.; Zhang, Y.; Nagel, R.; Reisner, W.; Dunbar, W. B. Controlling DNA Tug-of-War in a Dual Nanopore Device. *Small* **2019**, 15 (30), 1901704.
- [12] Liu, X.; Zimny, P.; Zhang, Y.; Rana, A.; Nagel, R.; Reisner, W.; Dunbar, W. B. Flossing DNA in a Dual Nanopore Device. *Small* **2020**, 16 (3), 1905379.
- [13] Bhattacharya, A.; Seth, S. Tug of War in a Double-Nanopore System. *Phys. Rev. E* **2020**, 101 (5).
- [14] Seth, S.; Bhattacharya, A. Polymer Escape through a Three Dimensional Double-Nanopore System. *J. Chem. Phys.* **2020**, 153 (10), 104901.
- [15] Choudhary, A.; Joshi, H.; Chou, H.-Y.; Sarthak, K.; Wilson, J.; Maffeo, C.; Aksimentiev, A. High-Fidelity Capture, Threading, and Infinite-Depth Sequencing of Single DNA Molecules with a Double-Nanopore System. *ACS Nano* **2020**, 14 (11), 15566-15576.
- [16] Sakaue, T. Nonequilibrium Dynamics of Polymer Translocation and Straightening. *Phys. Rev. E* **2007**, 76 (2).
- [17] Ikonen, T.; Bhattacharya, A.; Ala-Nissila, T.; Sung, W. Influence of Non-Universal Effects on Dynamical Scaling in Driven Polymer Translocation. *The Journal of Chemical Physics* **2012**, 137 (8), 085101.
- [18] Adhikari, R.; Bhattacharya, A. Driven Translocation of a Semi-Flexible Chain through a Nanopore: A Brownian Dynamics Simulation Study in Two Dimensions. *The Journal of Chemical Physics* **2013**, 138 (20), 204909.
- [19] Rubinstein, M.; Colby, R. H. *Polymer physics*. Oxford: Oxford University Press **2003**.
- [20] Grest, G. S.; Kremer, K. Molecular Dynamics Simulation for Polymers in the Presence of a Heat Bath. *Phys. Rev. A* **1986**, 33 (5), 3628-3631.
- [21] Binder, K. *Monte Carlo and Molecular Dynamics Simulations in Polymer Science*; Oxford University Press, **1995**, Chap. 2.
- [22] Huang, A.; Bhattacharya, A.; Binder, K. Conformations, Transverse Fluctuations, and Crossover Dynamics of a Semi-Flexible Chain in Two Dimensions. *The Journal of Chemical Physics* **2014**, 140 (21), 214902.
- [23] Huang, A.; Adhikari, R.; Bhattacharya, A.; Binder, K. Universal Monomer Dynamics of a Two-Dimensional Semi-Flexible Chain. *EPL* **2014**, 105 (1), 18002.
- [24] Huang, A.; Reisner, W.; Bhattacharya, A. Dynamics of DNA Squeezed Inside a Nanochannel via a Sliding Gasket. *Polymers* **2016**, 8 (10), 352.
- [25] Bernier, S.; Huang, A.; Reisner, W.; Bhattacharya, A. Evolution of Nested Folding States in Compression of a Strongly Confined Semiflexible Chain. *Macromolecules* **2018**, 51 (11), 4012-4022.
- [26] Landau, L. D.; Lifshitz, E. M. *Statistical Physics*; Pergamon Press **1981**.
- [27] van Gunsteren, W. F.; Berendsen, H. J. C. Algorithms for Brownian Dynamics. *Molecular Physics* **1982**, 45 (3), 637-647.